# Spin-dependent resonant quantum tunneling between magnetic nanoparticles on a macroscopic length scale

J. Varalda,[1] C. A. Dartora,[2] A. J. A. de Oliveira,[3] W. A. Ortiz,[3] B. Vodungbo,[4] M. Marangolo,[4] F. Vidal,[4] Y. Zheng,[4] G. G. Cabrera,[5] and D. H. Mosca[1]

[1]*Departamento de Física, Universidade Federal do Paraná, Caixa Postal 19044, 81531-990 Curitiba, Paraná, Brazil*
[2]*Departamento de Engenharia Elétrica, Universidade Federal do Paraná, Caixa Postal 19011, 81531-990 Curitiba, Paraná, Brazil*
[3]*Departamento de Física, Universidade Federal de São Carlos, Caixa Postal 676, 13565-905, São Carlos, São Paulo, Brazil*
[4]*Institut des NanoSciences de Paris, INSP, UPMC-Paris 6, CNRS UMR 7588, 4 place Jussieu, 75252 Paris Cedex 05, France*
[5]*Instituto de Física Gleb Wataghin, Universidade Estadual de Campinas, 13083-970 Campinas, São Paulo, Brazil*

Macroscopic quantum phenomena are common features observed in superconductors, superfluid helium, and Bose-Einstein condensates. However, most of quantum transport studies are based on a small number of dots and are not in long-range electron transport length scale. Here we show that spin-dependent resonant quantum tunneling is achieved in the macroscopic length scale (a few millimeters) corresponding to an array of up to $10^4$ junctions in a series consisting of Co nanoparticles embedded in an oxygen-deficient $TiO_2$ matrix. This phenomenon is observed by magnetoresistance measurements at 5 K in a Coulomb blockade regime. We further present a model based on resonant spin-polarized quantum tunneling of electrons of Co particles. It occurs through resonant continuous spin-polarized defect band states located near the Fermi level of the defective $TiO_2$, which acts as a magnetic tunnel barrier. These results might be potentially useful for future designs of spintronic quantum devices.

PACS number(s): 72.25.−b, 73.23.Hk, 73.40.Gk

## I. INTRODUCTION

Macroscopic quantum phenomena are studied by measurement of current-voltage ($I$-$V$) curves in stacks of intrinsic Josephson junctions (IJJs) that are generally patterned by lithography.[1–3] The switching dynamics of the IJJs is described by means of the time which the system spends in the superconducting state before decay toward another state. Despite the high-temperature superconductivity, the phenomenon is observed only at very low temperatures (below 1 K), where the tunnel effect prevails and quantum processes can be evidenced. The quantized energy levels in the stacked system composed of $N$ equivalent junctions have an energy distribution which can be manipulated or probed by microwave irradiation. The successive quantum tunneling on all the switching junctions has a characteristic escape rate proportional to $N^2$.[1,4] Macroscopic quantum tunneling of electrons is also studied in nanometer-scale semiconductor heterostructures consisting of superlattices[5] and quantum wells (QW),[6] which favors the invention of the multiple QW and QW cascade lasers. Nowadays, two-dimensional arrays of quantum dots connected to conducting leads by lithographic methods are also exploited for quantum computation applications.[7] However, most quantum transport studies are based on a small number of dots and are not in long-range electron transport scale,[8] because spin-polarized propagation, in the best cases, is limited to micrometric distances in semiconductors due to intrinsic relaxation processes.[9]

In the present work we report on spin-polarized current flow up to millimeter length scale in a nanostructured system. This phenomenon is achieved by spin-polarized resonant quantum tunneling in a planar array of magnetic nanoparticles embedded in a semi-insulating matrix. As we describe in detail below, the spin-polarized electron resonant tunneling occurs between discrete energy levels of nanosized Co particles through continuous spin-polarized defect states of the oxygen-deficient $TiO_2$ matrix which exhibits a ferromagnetic behavior, i.e., acts as a spin-filtering barrier.

The planar self-assembly of Co nanoparticles embedded in $TiO_2$ films was prepared using pulsed laser deposition. The growth conditions as well as structural and magnetic characterizations of these nanostructures are described elsewhere.[10,11]

## II. EXPERIMENT

Co clusters embedded in $TiO_2$ matrix have been prepared by pulsed laser deposition from metallic Co and nominal $TiO_2$ targets with a base pressure around $10^{-7}$ mbar. A pulsed excimer KrF laser ($\lambda = 248$ nm, pulse of 20 ns) was used at a fluence of about 3 J cm$^{-2}$ and a repetition rate of 2 Hz. The distance between the substrate and the target was 5 cm. First of all, a 40-nm-thick $TiO_2$ buffer layer was grown on the native thin oxide layer of a commercial Si(100) wafer. The Co granular film was grown at room temperature on the $TiO_2$ buffer layer, followed by a 40-nm-thick overlayer of $TiO_2$. Transmission electron microscopy analyses reveal that Co clusters have spherical shapes with diameters between 3 and 4 nm and intercluster distances of about 2 nm.[11] Magnetic measurements were carried out using a superconducting quantum interference device (SQUID) magnetometer (Quantum Design MPMS-5S) with the applied magnetic field parallel to the film surface. Direct current electric transport measurements were carried out in a Quantum Design PPMS-6000 system using standard two electric leads.

## III. RESULTS AND DISCUSSION

Figure 1 exhibits electric and magnetic characterizations of the samples. The differential conductance as a function of the bias voltage for steady magnetic fields of 0 and 10 kOe are
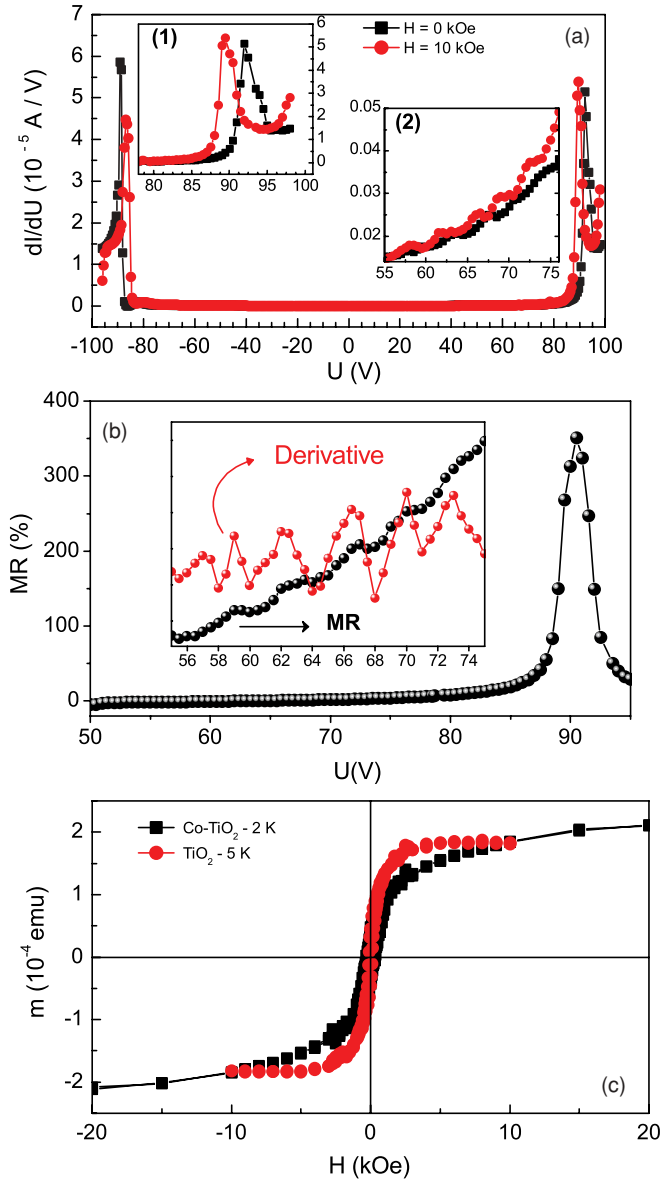
FIG. 1. (Color online) (a) Conductance curves as a function of voltage bias for $TiO_2$:Co films at magnetic fields of 0 and 10 kOe. Insets 1 and 2 show details of the conductance curves measured at 5 K. (b) Magnetoresistance (MR) as a function of voltage bias measured at 5 K. Inset shows details of the MR curve in the region of the Coulomb staircase, as well as of the MR derivative exhibiting clear oscillations related to the staircase. (c) M-H hysteresis loops measured at 5 K for a pure $TiO_2$ film and at 2 K for a $TiO_2$:Co film.

presented in Fig. 1(a). Up to a threshold value of voltage, a very small conductance is observed. The voltage conductance peak is dependent on the field value, as can be seen in Inset 1 of Fig. 1(a) for 0 and 10 kOe. Rather different conductance in the absence of a magnetic field and at an applied field of 10 kOe lead to the observation of high magnetoresistance, as shown in Inset 1. Inset 2 shows the existence of an equally spaced Coulomb staircase in the conductance curve. This Coulomb staircase is due to the large number of junctions and the almost monodisperse size distribution of Co nanoparticles which mimics discrete jumps of electrons as observed in

systems with fewer nanoparticles.[12] The sensitivity of the measurements is high enough to observe the Coulomb staircase in the magnetoresistance curve [see Fig. 1(b)]. Figure 1(c) shows magnetic hysteresis (M-H) loops found for a pure $TiO_2$ and for a $TiO_2$:Co film. Experimental observation of hysteresis loops for both samples indicates that ferromagnetism of the $TiO_2$ is superimposed to the superparamagnetism of the planar assembly of Co nanoparticles, as previously described.[10] Saturation magnetization of $TiO_2$:Co film is found to be $M_s = 54$ emu/cm$^3$, whereas $TiO_2$ film exhibits $M_s = 36$ emu/cm$^3$. The ferromagnetism of undoped $TiO_{2-x}$ films was recently reported[13] and described in terms of a spin-split defect-impurity band model.[14]

We describe the peaks in the conductance curves shown in Fig. 1(a) as resulting from a spin-polarized resonant tunneling mechanism. The resonant states are close to the Fermi level in the $TiO_2$ barrier formed between Co nanoparticle pairs along the current lines. To model this mechanism it was also taken into account the fact that discrete energy levels are expected in the Co particles due to its low dimensionality.[15] A single-particle estimate of the half-spin mean level spacing near the Fermi level for Co particles with a diameter of 4 nm is $\delta \sim 1.0$ meV.[10,16] Thus, the discrete levels are expected to be resolved for temperatures up to 10 K through the resonant tunneling. It is worth noting that at large magnetic fields the energy of a given state does not depend on the orientation of the magnetic moment produced by all the electrons within the particle, but these energy levels have a roughly linear dependence on applied $H$ due to the spin Zeeman energy with $H$ slope, having the same sign in each particle.[16,17] Concerning the resonant levels, the presence of oxygen vacancies forms a defect-impurity band located in the band gap just below the Fermi level $E_F$ in the case of an abrupt interface between metallic Co and reduced $TiO_2$.[18] These defect states are created by $Ti^{3+}$ (3$d$) ions and from an occupied half-spin Ti 3$d$ defect sub-band with estimated linewidth of about $\Sigma \sim 2$ eV (Ref. 19) for the oxygen deficiency ($x \sim 0.05$–0.10) found in our samples.[11] An empty Ti 3$d$ defect sub-band is formed in the conduction band, depending on the exchange splitting caused by charge transfer around two $Ti^{3+}$ ions near an O vacancy and the magnitude of applied magnetic field. Since the applied magnetic field breaks the symmetry of the spin-up and spin-down states in the Co particles it will presumably change the position of these discrete energy levels relative to the spin-down defect-impurity sub-band. The majority spin-down density of states (DOS) on each Co nanoparticle matches the spin-down impurity-defect states continuously spread out around the Fermi level. A schematic diagram of the resonant tunneling mechanism between discrete energy levels of two adjacent Co nanoparticles through impurity-defect band states of defective $TiO_2$ is shown in Fig. 2(a). The energy shifts induced by the applied magnetic field in the discrete and continuous energy levels are schematically represented in Fig. 2(b).

A consistent choice for the resonant current is a sequential model because (i) the phase breaking processes apparently have little effect on the resonant current[20] and (ii) at low temperatures and high bias the fully sequential model agrees precisely with that obtained from a fully coherent model for double junctions.[21] Thus, sequential resonant tunneling
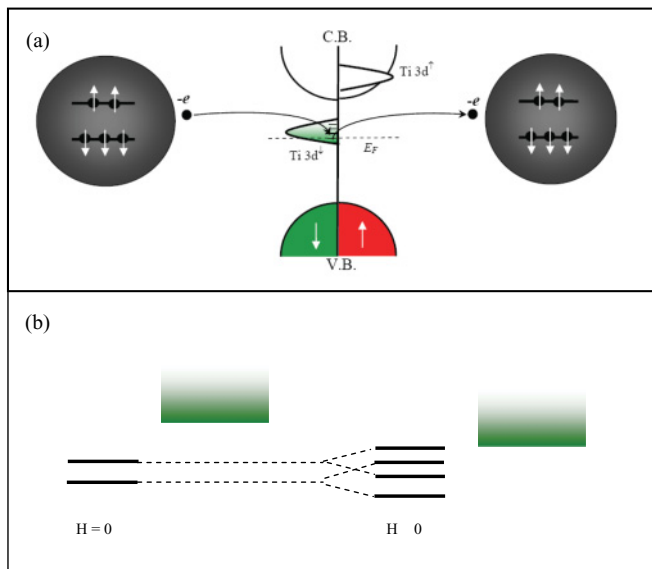
(a)

(b)

FIG. 2. (Color online) (a) Schematic diagram of resonant tunneling mechanism between discrete energy levels of two neighbor Co nanoparticles spaced by a reduced TiO$_2$ barrier. Resonant tunneling occurs via spin-down sub-band consisting of Ti 3$d$ levels formed near Fermi level $E_F$. An empty spin-up sub-band is located in the conduction band due to exchange splitting. The valence band (V.B) and the conduction band (C.B.) are both represented with parabolic shapes. (b) The influence of an applied magnetic field on the discrete and continuous energy levels is schematically represented. The energies are not in scale.

between Co nanoparticles is expected to occur predominantly through continuously spaced spin-down band states associated with Ti 3$d$ located near $E_F$. The total current can be obtained approximately by adding up the currents carried by all the resonant modes. A direct tunneling term is also expected. However, the direct tunneling of Co (majority or minority) spin electrons likely has a faster decaying that can depend on the symmetry selected by the electronic states in the TiO$_2$ barrier.

The experimental system is assumed as a planar array of monodisperse magnetic nanoclusters with average diameter $d$ and average cluster separation $s$ spaced by TiO$_2$ barriers. In this scenario, the exchange interaction between neighboring Co clusters is negligible and each cluster acts individually as a superparamagnet under the influence of an applied magnetic field. Since the typical band gap of TiO$_2$ is around 3.1 eV, it represents a high potential barrier with respect to the bias voltage and the electronic transport is dominated by spin-dependent tunneling phenomena. Under the influence of an applied magnetic field each magnetic Co cluster shows a strong magnetization and high spin polarization ($P_{Co} = 0.45$) with local band structure strongly dependent on spin. The tunneling transport is dominated by the $s$-like components of the wave functions while $d$-like components contribute in a significant manner only to local magnetization. Assuming that the Coulomb energy is higher than other involved energies, it is reasonable to assume that no more than one conduction electron is allowed in each metallic grain at a given instant. Considering the average diameter $d$ of each cluster of order

of 4nm immersed in the TiO$_2$ matrix having a relative dielectric constant $\varepsilon_r = 80$ and cluster to cluster separation $s \sim 3$ nm, we obtain the electrostatic Coulomb energy $U_c \approx e^2/(2\pi\varepsilon_0\varepsilon_r d)[s/(d/2 + s)]$ in the range of 5 meV. In this way, the electronic transport is described by a spin-dependent hopping Hamiltonian of the form

$$\mathcal{H}_T = \sum_{ik\sigma, jk'\sigma'} t_{ij}(k,k')\Gamma_{\sigma\sigma'}c^\dagger_{ik\sigma}c_{jk'\sigma'}, \qquad (1)$$

where $c^\dagger_{ik\sigma}$ and $c_{ik\sigma}$ are creation and annihilation electronic operators of spin $\sigma$, respectively, $t_{ij}(k,k')$ is the hopping energy, and the matrix $\Gamma$ represents the projection between the spin eigenstates of $i$th and $j$th clusters, being given by

$$\Gamma = \begin{pmatrix} \cos(\theta_{ij}/2) & \sin(\theta_{ij}/2) \\ -\sin(\theta_{ij}/2) & \cos(\theta_{ij}/2) \end{pmatrix}, \qquad (2)$$

where $\theta_{ij}$ is the relative angle between the magnetization of clusters $i$ and $j$. In the superparamagnetic state we are allowed to set $\theta_{ij} = \theta$ and work with the averaged value of $\cos^2(\theta/2)$, given by $\langle\cos^2(\theta/2)\rangle = \frac{1}{2}[1 + m^2(H)]$, with $m(H) = M(H)/M_s$ being the reduced magnetization.[22] The superparamagnetic function $M(H)$ can be represented by $M(H) = M_s\mathcal{L}(\beta\mu H)$, where $M_s$ is the saturation magnetization, $\mu$ is the total magnetic moment of a single cluster, $H$ is the applied magnetic field intensity, and $\mathcal{L}(x)$ is the Langevin function. The electronic current flowing through the system under the influence of a bias voltage can be evaluated by usual methods based on the scattering matrix $S = \mathcal{H}_T + \mathcal{H}_T G_0 S$,[23] where $G_0 = (\varepsilon - \mathcal{H}_0 + i\eta)^{-1}$ is the nonperturbed retarded Green's function, $\mathcal{H}_0$ is a nonperturbed Hamiltonian, and $\eta = \hbar/\tau$ is related to the mean lifetime $\tau$ of a given accessible state, even though there are several complications in an assembly having a large number of nanoclusters. The whole scenario can be understood from Fig. 3(a), which shows the possible paths that the conduction electron can follow in an array of $N_c \times N$ Cobalt grains embedded in the TiO$_2$ matrix when a voltage bias is applied to the sample through macroscopic electrodes. The main difficulty is related to the fact that conduction electrons can percolate and the number of possible paths in a matrix grow as $N_c^N$. However, we can take advantage of the physics of tunneling, which states that tunneling events between distant nanoclusters are exponentially dumped. The most probable path between two distant points will be the shortest path connecting them, since the probability $p_2$ for the electron tunnel from one site to a next-nearest neighbor is exponentially smaller than the tunneling probability $p_1$ between first nearest neighbors by a factor $\exp(-\delta)$, where $\delta$ is a parameter related to the distance between the Cobalt grains. The assembly can be modeled as an appropriate association of series and parallel resistors representing the different transport mechanisms. In our analysis we consider the assembly as an appropriate association of $N_c$ parallel resistors representing the straightest paths between the two electrodes, each resistor containing $N$ tunneling junctions in series. Thus only $N_c$ parallel paths are considered, as contrasted to the total number $N_c^N$ of possible paths. We note, however, that paths deviating slightly from the shortest ones may contribute to the total current; therefore
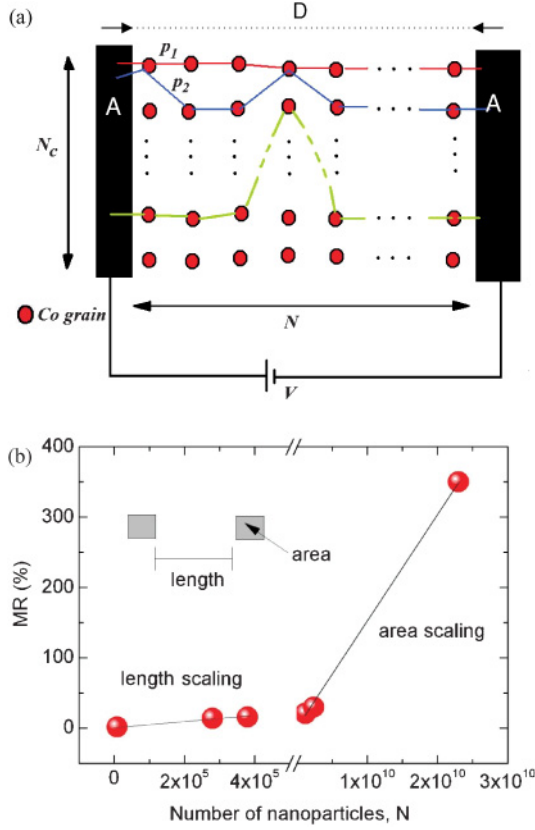
FIG. 3. (Color online) (a) Schematic representation of electron tunneling paths between leads with area A separated by a distance $D$. (b) Maximal MR values scale with the number of Co nanoparticles along the length between electric contacts with fixed area (200 $\mu$m × 200 $\mu$m) as well as with the number of Co nanoparticles below the area of the electrical leads held at a fixed distance (3000 $\mu$m).

our approximation somewhat overestimates the current in the most probable paths.

We can thus model the assembly as an appropriate association of resistors representing different transport mechanisms. The first-order process connects two neighboring clusters $i$ and $j = i + 1$ with the voltage difference between them approximately given by $V/N$, with $V$ being the bias voltage and $N$ being the number of tunnel junctions connected in series in the straightest path linking the two electrodes. The current between two nearest neighbors $i$ and $j = i + 1$ is shown to be

$$I(V/N) = \frac{2\pi e^2}{\hbar} \sum_{\sigma\sigma'} \int d\varepsilon\, T_{\sigma\sigma'}(\varepsilon) D_{i\sigma'}(\varepsilon) D_{j\sigma}(\varepsilon)$$
$$\times [f_i(\varepsilon) - f_j(\varepsilon + eV/N)] \exp[-\beta(U_c - \varepsilon)], \quad (3)$$

in which $D_{i\sigma}(\varepsilon)$ is the $i$th cluster spin-$\sigma$ DOS at energy $\varepsilon$, $f(\varepsilon) = (1 + e^{\beta\varepsilon})^{-1}$ is the Fermi-Dirac function, the exponential $e^{-\beta(U_c-\varepsilon)}$ is a Maxwell-Boltzmann probability distribution related to the Coulomb blocking phenomena, $\beta = (k_B T)^{-1}$ is the reciprocal of the thermal energy given by product of the absolute temperature $T$ and Boltzmann constant $k_B$, and $T_{\sigma\sigma'} = |\langle\sigma'|S|i\sigma\rangle|^2$ is the spin-dependent tunneling coefficient, given in the low-bias regime by the approximation

below (i.e., a generalization of Breit-Wigner formula):

$$T_{\sigma\sigma'}(\varepsilon) \approx T_0 \exp(\alpha\varepsilon)|\Gamma_{\sigma\sigma'}|^2 \left[1 + \frac{A_{\sigma\sigma'}}{[\varepsilon - \beta_{\sigma\sigma'}]^2 + \eta_{\sigma\sigma'}^2}\right], \quad (4)$$

where $A_{\sigma\sigma'} \propto D_\sigma^{\text{TiO}_2}|\Gamma_{\sigma\sigma'}|^2$ is a parameter proportional to the DOS of the virtual resonant levels inside the barrier, $D_\sigma^{\text{TiO}_2}$, and to a spin-dependent scattering matrix similar to Eq. (2) measuring the alignment of the cobalt grain magnetization relative to an allowed state inside the barrier; reflecting the magnetic behavior of the barrier, $\beta_{\sigma\sigma'} = \beta_{\sigma\sigma'}(H)$ is the resonant level inside the TiO$_2$, being the splitting of this energy level controlled by the applied magnetic field; and $\eta_{\sigma\sigma'}$ is the mean transit time of the electron. The constants $T_0 = \tau_0 e^{-2\alpha V_0}$ represents a scaling factor, in which $\alpha = \sqrt{2m_e s^2/(\hbar^2 V_0)}$ is easily obtained from the WKB approximation, $V_0$ being the barrier height, $m_e$ the effective electron mass, and $s$ the distance between neighboring clusters. For typical barrier heights in the range of 3 eV for oxide insulating barriers we can make $e^{\alpha\varepsilon} \to 1$ and neglect variations in the DOS at very low bias. Also, at low temperatures the Fermi-Dirac functions are steplike. In the following, we introduce a rescaling of the energy represented by the relation $E = N\varepsilon$, in such a way that new rescaled parameters are in order, being given by $\kappa = \beta/N$, $B_{\sigma\sigma'} = N^2 A_{\sigma\sigma'}$, $\Sigma_{\sigma\sigma'} = N\beta_{\sigma\sigma'}$, and $\gamma_{\sigma\sigma'} = N\eta_{\sigma\sigma'}$. The striking consequence of the rescaling of the parameters by a factor $N$ is that a small energy difference $\delta E$ in the levels of a single cluster manifests itself as a factor $N \times \delta E$. For simplicity, we introduce by hand into the Eq. (3) a numerical factor $N_c$ corresponding to the fact that there exists $N_c$ parallel lines of current containing $N$ tunneling junctions in series for each one. In practice, only spin-down resonant electronic levels due to defects inside the TiO$_2$ barrier are accessible at the bias voltages being considered. For the sake of simplicity, we are assuming that $\gamma_{\sigma\sigma'} = \gamma$, independent of spin and applied magnetic field. In such a case, a general expression for the current in terms of the relative reduced magnetization between two Co grains, $m(H)$, and between Co grains and the TiO$_2$ matrix, $m'(H)$, is given below:

$$I(H,V) = \frac{2\pi e^2 N_c T_0 e^{-\beta U_c}}{N\hbar}[F_d(H,V) + F_r(H,V)], \quad (5)$$

where the direct and resonant tunneling functions, $F_d$ and $F_r$, respectively, are defined as

$$F_d(H,V) = \{(1 + r^2)\Lambda_+(H) + 2r\Lambda_-(H)\}(e^{\kappa V} - 1), \quad (6)$$

$$F_r(H,V) = \{r^2\Lambda_+(H)\Lambda'_+(H) + \Lambda_-\Lambda'_-(H)$$
$$+ r[\Lambda_+(H)\Lambda'_-(H) + \Lambda_-(H)\Lambda'_+(H)]\}J_r, \quad (7)$$

where the $\Lambda$ functions are defined as $\Lambda_\pm(H) = \frac{1}{2}[1 \pm m^2(H)]$ and $\Lambda'_\pm(H) = \frac{1}{2}[1 \pm m'^2(H)]$; $r = D_\uparrow/D_\downarrow = (1 + P)/(1 - P)$ is the majority to minority spin bands ratio, with $D_\uparrow$ and $D_\downarrow$ being the DOS for majority and minority local spin bands for the Co nanoparticles, respectively; $P$ is the spin band polarization; and the other functions are defined as

$$J_r(H,V) = \int_0^V \frac{B_0 e^{\kappa E}}{[E - \Sigma(H)]^2 + \gamma^2} dE, \quad (8)$$

$$\Sigma(H) = N\{\epsilon_0 - \mu_B[H + 4\pi M_s m(H)]\}, \quad (9)$$

where $\varepsilon_0$ is the spin-down resonant peak energy level inside the barrier and $\mu_B$ is the Bohr magneton. Notice that the resonant level at the barrier moves relative to the energy of the tunneling electrons with the applied magnetic field $H$.

As in standard experiments to observe the MR, one compares the electronic current flowing through the sample in two situations: (i) absence of applied magnetic field, $H = 0$, and (ii) in the presence of a saturating applied magnetic field, $H = H_s$, high enough to give $M(H) = M_s$. By accounting for the aforementioned assumptions, we are able to interpret the physics of tunneling as follows: In the absence of an externally applied magnetic field, $H = 0$, the relative angle $\theta$ of the spin quantization axis of the cobalt grains and the barrier levels are randomly oriented due to thermalization. The mean value of $\langle \cos^2(\theta/2) \rangle = [1 + m^2(H)]/2$ tends to $\langle \cos^2(\theta/2) \rangle_0 \rightarrow 1/2$ for the vanishing applied field. By contrast, in the presence of a saturating magnetic field, $H = H_s$, there is a tendency for the spin bands to align, giving $\langle \cos^2(\theta/2) \rangle_H = 1$, thus forbidding the tunneling of spin-up channels through a resonant process, if we assume that the barrier magnetization has already reached saturation. Taking the following definition for the MR ratio,

$$\text{MR} = \frac{I(H,V) - I(0,V)}{I(0,V)} = \frac{I(H,V)}{I(0,V)} - 1, \qquad (10)$$

it is a straightforward matter to show that in the limit of sharp resonance width, corresponding to $\gamma \rightarrow 0$ the Lorentzian function inside expression (8) tends to a Dirac $\delta$ function, leading us to the maximum value of the MR:

$$\text{MR}_{\text{max}} \approx P^2 \left[ 1 + \frac{2\pi r^2 B_0}{(r-1)^2 \gamma} e^{-\kappa(\Sigma_0 - \Sigma_H)} \right], \qquad (11)$$

which occurs for bias voltage values in the range $\Sigma_H < eV < \Sigma_0$. Since the factor $B_0$ scales with $N^2$ and $\gamma$ with $N$, we observe that the maximum MR value has a linear dependence with respect to the number of series junctions, $\text{MR} = c_1 + c_2 N$, where $c_1$ and $c_2$ are constants. Actually this kind of relationship is encountered in experimental behavior, as shown in Fig. 3(b). It is noteworthy that the MR scales with the number of junctions (or nanoclusters) in between contacts as well as with the number of junctions traversed by current lines.

To compare our theory with the experimental data we selected the region of bias voltages in the range of 50–100 V, which corresponds to typical values of a few millivolts for magnetic tunnel junctions.

Figure 4 shows a comparison between simulations and experimental data for the currents in the parallel ($H = H_s$) and antiparallel ($H = 0$) configurations.

Figure 5 exhibits a comparison between theoretical predictions and experimental MR values as a function of applied bias voltage. A good agreement between simulation and experimental data is found. A MR value of about 20% is observed at low bias in the direct tunnel regime, whereas a MR value of 350% is obtained near the bias voltage of $V = 90$ V. We have used the following parameters to fit the curves: the majority to minority spin DOS ratio typical for Co is $r = 2.6$, corresponding to a spin band polarization of the order of $P \approx 45\%$; $B_0 = 2 \,(\text{eV})^2$ is related to the DOS of spin-down resonant
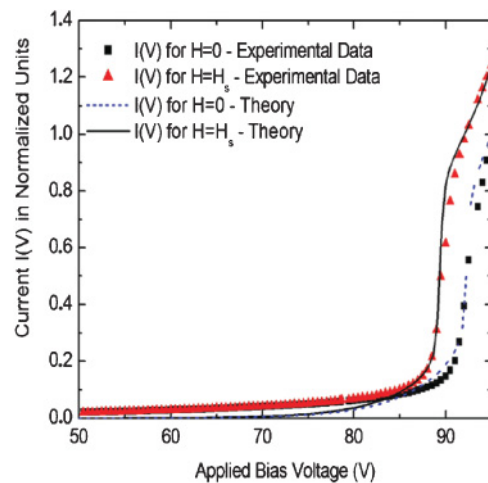


FIG. 4. (Color online) Comparison between the experimental and theoretical curves for the current $I(V)$ as a function of the applied bias voltage for the parallel ($H = H_s$) and antiparallel ($H = 0$) configurations. Theoretical curves were obtained from expressions (5)–(9). The values of the relevant parameters are given throughout the text.

levels; the resonance width is chosen to be $\gamma = 0.26$ eV; and the resonant energies for a good adjustment between theoretical and experimental data are $\Sigma(0) = 92.3$ eV, $\Sigma(H_s = 10 \,\text{kOe}) = 89.4$ eV, and $\kappa = 0.1784 \,(\text{eV})^{-1}$ at $T = 5$ K, which allows one to obtain $N \approx 1.31 \times 10^4$ series junctions and the saturation magnetization $M_s = 2280$ emu/cm$^3$ for Co grains, which corresponds to approximately $8200 \,\mu_B$. This value is close to $10\,000 \,\mu_B$ estimated from Langevin fittings of $M(H)$ curves for Co grains having a spherical volume of 4 nm in diameter. The energy shift due to an applied magnetic field is in the range of 1 eV in $N$ junctions, which gives a splitting of order of 1 eV/$N \sim 50 \,\mu$eV. The value found for $\gamma = 0.26$ eV gives an estimate for the parameter $\eta = \gamma/N = 20 \,\mu$eV. This parameter represents the width of energy levels in Co grains in the Coulomb blockade regime, since the TiO$_2$ barrier mimics a continuum of resonant states. This value is in good agreement
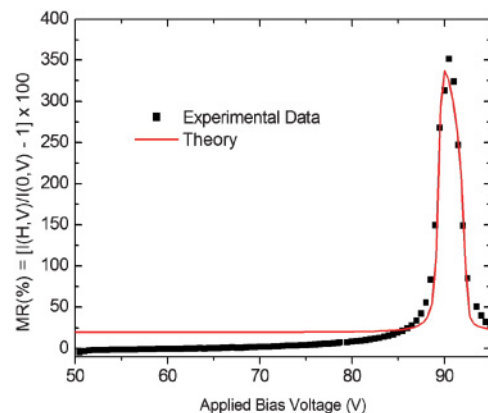


FIG. 5. (Color online) Comparison between the experimental and theoretical curves for the MR as a function of the applied bias voltage obtained from the parallel ($H = H_s$) and antiparallel ($H = 0$) configurations. The theoretical curve was obtained from expression (10).
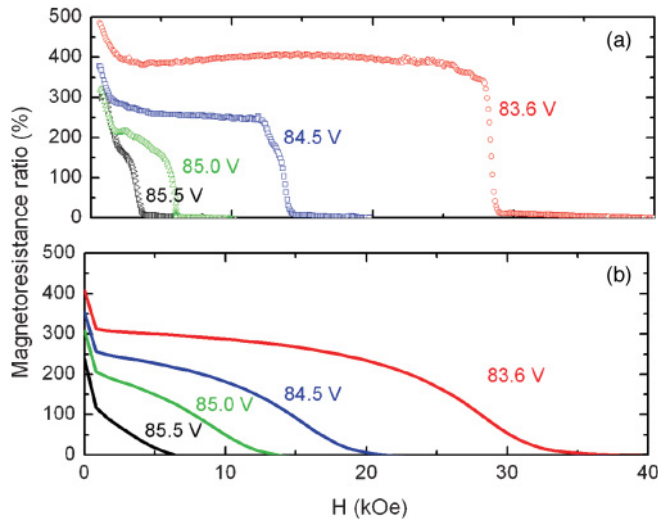
FIG. 6. (Color online) Experimental (a) and simulated (b) MR curves as a function of the applied magnetic field for some selected bias voltages, which are indicated along the curves.

with the data in Refs. 10 and 16. From the value of $\Sigma(0)$ we obtain the resonant level inside the barrier, which is given by $\epsilon_0 = \Sigma(0)/N = 7.1$ meV. Therefore, simulation results of $I(0,V)$ and $I(H,V)$ curves are in quite good agreement with experiments using reasonable values for the physical parameters involved.

In order to check the validity of our model we also present in Figs. 6(a) and 6(b) the saturation branches of MR curves and our theoretical simulations. The MR peak is near 84.3 V in this case due to a small number of Co nanoparticles along the length between electric contacts. The best fit is obtained by choosing an effective number of series junctions equal to $N = 1.24 \times 10^4$, while the other parameters are kept the same, i.e., $r = 2.6$, $\eta = \gamma/N = 20$ $\mu$eV, $B_0 \approx 2$ (eV)$^2$, $\epsilon_0 = 7.1$ meV, and $M_s = 2280$ emu/cm$^3$. The initial resistance change is due to progressive alignment of the Co cluster magnetic moments

at low fields, which is followed by plateaus of resistance before switching to a lower saturation resistance value. The plateaus of resistance occur for bias voltage values near resonance in such a way that the additional energy contribution driven by the magnetic field tunes into resonance the discrete energy levels of Co cluster with defect levels in the TiO$_2$ barrier. At this point, the resistance switching occurs. Lower voltages imply in higher magnetic field values to achieve resonance and vice versa. The abrupt switching of resistance is difficult to model in detail. The complex phenomena involved in the relative energy shifts with magnetic fields, as described in Ref. 16, need further experimental investigations. Nevertheless, our present model is still able to reproduce the main features of the MR curves.

## IV. CONCLUSIONS

In summary, we demonstrated that a two-dimensional planar array of a large number of metallic nanoparticles embedded in an insulating matrix behaves as a simple artificial resonant tunneling structure working over a macroscopic length scale. The conductance and magnetoresistance curves were consistently simulated at low temperatures as a function of bias voltage and applied magnetic field by introducing a spin-filter term in the model. The relative alignment between the magnetizations of Co nanoclusters and barrier precedes and determines the onset of resonance by voltage and magnetic field originating the very high magnetoresistance observed. Our present results might be suitable for design and development in the not-too-distant future of spin-based resonant tunneling devices.

[1] S. Savelev, A. L. Rakhmanov, and F. Nori, Phys. Rev. Lett. **98**, 077002 (2007).

[2] X. Y. Jin, J. Lisenfeld, Y. Koval, A. Lukashenko, A. V. Ustinov, and P. Müller, Phys. Rev. Lett. **96**, 177003 (2006).

[3] K. Inomata, S. Sato, K. Nakajima, A. Tanaka, Y. Takano, M. Nagao, H. B. Wang, M. Hatano, and S. Kawabata, Phys. Rev. Lett. **95**, 107005 (2005).

[4] K. Inomata, S. Sato, M. Kinjo, N. Kitabatake, H. B. Wang, T. Hatano, and K. Nakajima, Supercond. Sci. Technol. **20**, S105 (2007).

[5] S. Takagi, *Macroscopic Quantum Tunneling* (Cambridge University Press, Cambridge, UK, 2002).

[6] R. Dingle, W. Wiegmann, and C. H. Henry, Phys. Rev. Lett. **33**, 827 (1974).

[7] See M. R. Astley, M. Kataoka, C. J. B. Ford, C. H. W. Barnes, D. Anderson, G. A. C. Jones, I. Farrer, D. A. Ritchie, and M. Pepper, Phys. Rev. Lett. **99**, 156802 (2007), and references therein.

[8] A. D. Yoffe, Adv. Phys. **50**, 1 (2001).

[9] R. Hanson and D. D. Awschalom, Nature (London) **453**, 1043 (2008).

[10] J. Varalda, W. A. Ortiz, A. J. A. de Oliveira, B. Vodungbo, Y.-L. Zheng, D. Demaille, M. Marangolo, and D. H. Mosca, J. Appl. Phys. **101**, 014318 (2007).

[11] B. Vodungbo, Y. Zheng, M. Marangolo, D. Demaille, and J. Varalda, J. Phys. Condens. Matter **19**, 116205 (2007).

[12] K. Yakushiji, S. Mitani, F. Ernut, K. Takanashi, and H. Fujimori, Phys. Rep. **451**, 1 (2007).

[13] S. Zhou, E. Cizmar, K. Potzger, M. Krause, G. Talut, M. Helm, J. Fassbender, S. A. Zvyagin, J. Wosnitza, and H. Schmidt, Phys. Rev. B **79**, 113201 (2009).

[14] J. M. D. Coey, M. Venkatesan, and C. B. Fitzgerald, Nat. Mater. **4**, 173 (2005).

[15] D. C. Ralph, C. T. Black, and M. Tinkham, Phys. Rev. Lett. **74**, 3241 (1995).

[16] S. Kleff, J. von Delft, M. M. Deshmukh, and D. C. Ralph, Phys. Rev. B **64**, 220401 (2001).

[17]S. Gueron, Mandar M. Deshmukh, E. B. Myers, and D. C. Ralph, Phys. Rev. Lett. **83**, 4148 (1999).

[18]Y. Shao, W. Chen, E. Wold, and J. Paul, Langmuir **10**, 178 (1994).

[19]Abdul K. Rumaiz, B. Ali, A. Ceylan, M. Boggs, T. Beebe, and S. I. Shah, Solid State Commun. **144**, 334 (2007).

[20]T. Weil and B. Vinter, Appl. Phys. Lett. **50**, 1281 (1987).

[21]S. Datta, *Electronic Transport in Mesoscopic Systems*, Cambridge Studies in Semiconductor Physics and Microelectronic Engineering Series (Cambridge University Press, Cambridge, UK, 2003).

[22]J. Inoue and S. Maekawa, Phys. Rev. B **53**, R11927 (1996).

[23]C. A. Dartora and G. G. Cabrera, Phys. Lett. A **334**, 46 (2005).